IEEE 2000 International Conference on Robotics and Automation,San Francisco, CA, April, 2000.

Dynamic Simulation for Grasping and Whole Arm Manipulation

Peng Song Masahito Yashima Vijay Kumar
General Robotics, Automation, Sensing and Perception (GRASP) Laboratory
University of Pennsylvania, 3401 Walnut Street, Philadelphia, PA 19104
E-mail: {pengs, yashima, kumar}@grip.cis.upenn.edu

Abstract

We propose a novel approach to dynamic simulation of grasps that overcomes difficulties due to inconsistencies in the forward dynamics problem. The key idea in the paper is a minimalist model of the contact compliance and the use of this model in situations when the performance of the rigid body model is not satisfactory. Our general framework allows for on-line diagnostics that enable the automatic switching between models to maximize efficiency while avoiding ambiguous situations. We illustrate the basic ideas by simulating the dynamics of several whole arm grasps.

1 Introduction

The ability to predict the dynamic behavior of a grasp with a given dynamic model and the control algorithms is critical to the design and analysis of multifingered grippers, legged locomotion systems, multi-arm systems, and other constrained robot systems [6, 11]. The dynamic analysis and the simulation (the prediction of motion given the external forces and moments on the system) of such systems is central to the design of such systems and the development of control algorithms [3, 16]. In the forward dynamics problem, it is well-known that in the frictionless case there is always a unique solution for the accelerations. When the constraints are not all independent, the system is statically indeterminate and the constraint forces cannot be uniquely determined [7, 15, 13]. In the frictional case, if the Coulomb frictional model is adopted, then the dynamics are more complicated. If all contacts are known to be rolling (sticking), then the relative tangential velocity is zero at each contact, and the existence of a solution can be shown if the constraints are independent [13]. In all other cases, the initial value problem can be shown to have no solution or multiple solutions for special choices of initial conditions [7, 8].

Recently, there has been some attention in the robotics community on overcoming these shortcomings by using rigid body models to predict the gross motion while using compliant contact models to predict the contact forces and the local deformations [5]. For example, a continuum model for modeling the deformations at each contact is described in [15]. Each contact is modeled as frictional elastic or viscoelastic, and the contact force distribution across the contact patch is calculated using a finite-element mesh [4, 14, 15]. Existence and uniqueness can be shown for the special case in which the maximum tangential force at each point is *a priori* known [4]. In contrast, Mirtich *et al.* [10] propose efficient, approximate algorithms for "impulsive dynamic simulation" that incorporate approximate impact models for collisions, thus trading off accuracy for efficiency. An explicit model of the contact compliance [2, 5] also allows the analysis of statically indeterminate grasps. Of course such contact models tend to be more complex and the parameters are more difficult to identify. Further, it is harder to simulate systems in which the time scale for the dynamics of contact interactions is significantly different from the time scale of rigid body dynamics [9, 12].

The compliant contact model, while resolving the difficulties with the forward dynamics problem, can result in a high-dimensional, stiff system of equations and a run time that is unacceptable for real-time simulation. The simplicity and efficiency of rigid body models, on the other hand, provide strong motivation for their use during those portions of a simulation when the rigid body solution is unique and stable [12]. In this paper, we combine the positive aspects of both models and develop an integrated approach to dynamic simulation. We use a rigid body dynamic model whenever appropriate guarantees of accuracy are available, and switch to a compliant contact model in other cases. This is illustrated through examples of whole arm grasps.

2 Models

2.1 Rigid body dynamics

We consider a system of multiple rigid effectors operating on rigid objects subject to Coulomb's friction as shown in Figure 1. The dynamic equations of motion can be written as

$$\boldsymbol{M}(\boldsymbol{q})\ddot{\boldsymbol{q}} + \boldsymbol{h}(\boldsymbol{q}, \dot{\boldsymbol{q}}) = \boldsymbol{u} + \boldsymbol{W}\boldsymbol{\lambda} \tag{1}$$

where $\boldsymbol{q} \in \Re^n$ is the vector of generalized coordinates, $\boldsymbol{M}(\boldsymbol{q})$ is an $n \times n$ positive-definite symmetric inertia matrix, $\boldsymbol{h}(\boldsymbol{q}, \dot{\boldsymbol{q}})$ is a $n \times 1$ vector of nonlinear inertial forces, $\boldsymbol{u}$ is the vector of applied (external) forces and torques, and $\boldsymbol{\lambda}$ is the vector of constraint forces. The system is subject to k unilateral constraints:

$$\boldsymbol{\phi}(\boldsymbol{q}) = [\phi_1(\boldsymbol{q}), \cdots, \phi_k(\boldsymbol{q})]^T \geq 0 \tag{2}$$

and $\boldsymbol{W}$ in Eq.(1) is the $k \times n$ Jacobian matrix, $(\frac{\partial \boldsymbol{\phi}}{\partial \boldsymbol{q}})^T$. We will assume, without loss of generality, that this does not include bilateral, holonomic constraints. Further, for the sake of simplicity, we will assume that nonholonomic constraints are not present.

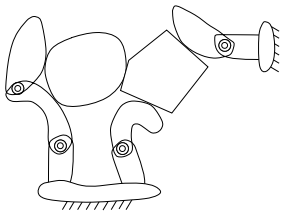

Figure 1: A general whole arm grasp.

Suppose there are n_C contacts, consisting of n_R rolling contacts and n_S sliding contacts. Let the subscripts N and T denote quantities in the normal and tangential contact directions and S and R denote sliding and rolling contacts respectively. The Jacobian matrix and constraint forces in Eq.(1) are given by:

$$\begin{aligned} \boldsymbol{W} &= [\boldsymbol{W}_{NR}\ \boldsymbol{W}_{TR}\ \boldsymbol{W}_{\mu}], \qquad (3) \\ \boldsymbol{W}_{\mu} &= [\boldsymbol{W}_{NS} + \boldsymbol{W}_{TS}\boldsymbol{\mu}_s], \\ \boldsymbol{\lambda} &= \left[\boldsymbol{\lambda}_{NS}^T\ \boldsymbol{\lambda}_{NR}^T\ \boldsymbol{\lambda}_{TR}^T\right]^T, \qquad (4) \end{aligned}$$

where $\boldsymbol{\mu}_s = -diag(\boldsymbol{\mu}\, sign(\dot{\boldsymbol{\phi}}_{TS}))$, $\boldsymbol{\mu}$ is a $n_S \times n_S$ diagonal matrix that contains all the coefficients of friction at the sliding contacts, $\boldsymbol{W}_{\mu}$ is a $n \times n_S$ matrix, $\boldsymbol{W}_{NR}$ and $\boldsymbol{W}_{TR}$ are both $n \times n_R$ matrices, and the total number of constraints $k = 2n_R + n_S$. $\boldsymbol{\lambda}_{NS}$ is the n_S-dimensional vector of normal forces at sliding contacts, while $\boldsymbol{\lambda}_{NR}$ and $\boldsymbol{\lambda}_{TR}$ are the $n_R \times 1$ vectors of normal and tangential forces at rolling contacts, respectively.

Contacts between rigid bodies generate complementary constraints on the position (or velocity or acceleration) variables and the corresponding force variables. The question of whether there exists a unique solution for $\ddot{\boldsymbol{q}}$ that is consistent with these constraints and Equations (1 - 4) and has been studied using complementarity formulations [7, 13]. The problem of determining contact forces can be reduced to a linear complementarity problem (LCP) that has the form [13]:

$$\boldsymbol{x} \geq 0,\ \boldsymbol{y} = \boldsymbol{A}\boldsymbol{x} + \boldsymbol{b} \geq 0,\ \boldsymbol{y}^T\boldsymbol{x} = 0. \qquad (5)$$

The LCP has a unique solution for all vectors $\boldsymbol{b}$ if and only if the matrix $\boldsymbol{A}$ is a P-matrix [1]. However, even if $\boldsymbol{A}$ is not a P-matrix, the LCP may have unique solution for special choices of $\boldsymbol{b}$. For other choices of $\boldsymbol{b}$, Eq.(5) may have no solution or multiple solutions.

2.2 Compliant contact models

The basic idea of the compliant contact model is shown in Figure 2, where the rigid body is shown surrounded by a very thin deformable layer the inertia of which is considered to be negligible. In the planar case, the actual relative displacement of the contact point is given by $(\boldsymbol{\phi}_T + \boldsymbol{\delta}_T, \boldsymbol{\phi}_N + \boldsymbol{\delta}_N)$, which is the summation of the relative rigid body displacement at the contact point, $(\boldsymbol{\phi}_T,\ \boldsymbol{\phi}_N)$, and the normal and tangential deformations of the deformable layer, $(\boldsymbol{\delta}_N, \boldsymbol{\delta}_T)$. The contact forces are related to the deformations $(\boldsymbol{\delta}_N, \boldsymbol{\delta}_T)$, and their derivatives $(\dot{\boldsymbol{\delta}}_N, \dot{\boldsymbol{\delta}}_T)$. Because the deformations can be determined by the knowledge of the material properties of the deformable layer, the contact forces can be related to the original state variables $(\boldsymbol{q}, \dot{\boldsymbol{q}})$.

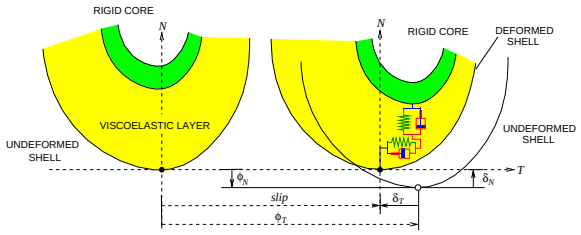

Figure 2: A simple model of contact compliance.

A general viscoelastic model for contact compliance is shown in Figure 2. At contact i, the normal and tangential contact forces ($\lambda_{N,i}$ and $\lambda_{T,i}$) between the two contacting bodies may be modeled as:

$$\lambda_{N,i} = f_{N,i}(\delta_{N,i}) + g_{N,i}(\delta_{N,i}, \dot{\delta}_{N,i}),\ i = 1, \ldots, n_C, \qquad (6)$$

$$\lambda_{T,i} = f_{T,i}(\delta_{T,i}) + g_{T,i}(\delta_{T,i}, \dot{\delta}_{T,i}),\quad i = 1, \ldots, n_C, \qquad (7)$$

where the functions $f_{N,i}$ and $f_{T,i}$ are the elastic stiffness terms and $g_{N,i}$ and $g_{T,i}$ are the damping terms in the normal and tangential directions respectively. These functions depend on the geometry and material properties of the two bodies in contact and may be nonlinear. It is also necessary to model the frictional behavior of the contact. The details and variations on the compliant contact model and a range of frictional laws are discussed in [5, 12].

The disadvantage of the compliant contact model is that there is a need to extend the dimension of the state space from $2n - 2(n_C + n_R)$ to $2n + n_C$. The three main advantages are: (a) The normal and tangential forces are now uniquely determined and there is no question of static indeterminacy; (b) The difficulties with uniqueness and existence no longer arise; and (c) A model with tangential contact compliance is more realistic and can better explain physical observations [5].

3 Planar whole arm manipulation

3.1 Dynamic model

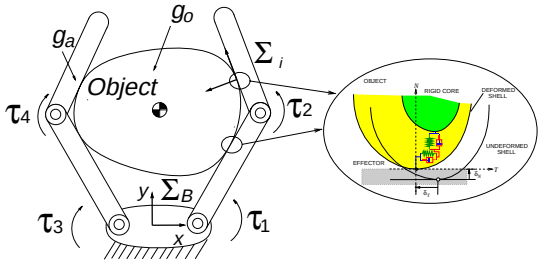

Figure 3: A planar whole arm grasp.

Consider the planar whole arm manipulation system shown in Figure 3. We assume that each link of each arm

(finger) has one contact point with the object. These links are called effectors. Each joint has one degree of freedom. Σ_B is the base frame and Σ_i is the coordinate frame attached to the ith contact point. Let T axis of Σ_i be aligned with the tangent to the object's surface, while the N axis is in the direction of the inward normal.

The generalized coordinates can be chosen as $\boldsymbol{q} = [\boldsymbol{x}^T \ \boldsymbol{\Theta}^T]^T \in \Re^7$, where $\boldsymbol{x} \in \Re^3$ describes the position and orientation of object and $\boldsymbol{\Theta} \in \Re^4$ be the joint angle of the robot manipulator. We define $\boldsymbol{G}_{N,i}$ and $\boldsymbol{G}_{T,i} \in \Re^3$ as the unit wrenches associated with contact forces $\lambda_{N,i}$ and $\lambda_{T,i}$ respectively. Let $\boldsymbol{J}_N^T$ and $\boldsymbol{J}_T^T \in \Re^{4\times 4}$ be the arm Jacobians which map the normal and tangential contact wrenches to the joint torque $\boldsymbol{\tau} \in \Re^4$. If Coulomb's friction law is assumed, the dynamics of the system in Figure 3 can be written in the form of Eqs.(1-4) as:

$$\begin{bmatrix} \boldsymbol{M}_o & 0 \\ 0 & \boldsymbol{M}_a \end{bmatrix} \begin{bmatrix} \ddot{\boldsymbol{x}} \\ \ddot{\boldsymbol{\Theta}} \end{bmatrix} + \begin{bmatrix} 0 \\ \boldsymbol{h}_a \end{bmatrix} = \begin{bmatrix} \boldsymbol{g}_o \\ \boldsymbol{\tau} - \boldsymbol{g}_a \end{bmatrix} + \boldsymbol{W} \begin{bmatrix} \boldsymbol{\lambda}_{NR} \\ \boldsymbol{\lambda}_{TR} \\ \boldsymbol{\lambda}_{NS} \end{bmatrix} \quad (8)$$

where $\boldsymbol{W} \in \Re^{7\times(2n_R+n_S)}$ is given by Eq.(3) with

$$\begin{aligned} \boldsymbol{W}_N^T &= [\boldsymbol{G}_N^T \ \ -\boldsymbol{J}_N] \in \Re^{4\times 7}, \\ \boldsymbol{W}_T^T &= [\boldsymbol{G}_T^T \ \ -\boldsymbol{J}_T] \in \Re^{4\times 7}. \end{aligned}$$

$\boldsymbol{M}_o$ is the mass matrix of the object. $\boldsymbol{M}_a \in \Re^{4\times 4}$ is inertia matrix of the arm. The vector $\boldsymbol{g}_o$ denotes the external wrench acting on the object. $\boldsymbol{h}_a \in \Re^4$ is the vector of Coriolis and centrifugal forces, and $\boldsymbol{g}_a \in \Re^3$ represents the vector of generalized forces that accounts for external forces acting on the arm. The kinematic constraints on velocities and accelerations are given by

$$\dot{\phi}_N = \boldsymbol{W}_N^T \dot{\boldsymbol{q}}, \quad \dot{\phi}_T = \boldsymbol{W}_T^T \dot{\boldsymbol{q}}. \quad (9)$$

$$\begin{bmatrix} \ddot{\phi}_{NR} \\ \ddot{\phi}_{TR} \\ \ddot{\phi}_{NS} \end{bmatrix} = \begin{bmatrix} \boldsymbol{W}_{NR}^T \\ \boldsymbol{W}_{TR}^T \\ \boldsymbol{W}_{NS}^T \end{bmatrix} \ddot{\boldsymbol{q}} + \begin{bmatrix} \dot{\boldsymbol{W}}_{NR}^T \\ \dot{\boldsymbol{W}}_{TR}^T \\ \dot{\boldsymbol{W}}_{NS}^T \end{bmatrix} \dot{\boldsymbol{q}}. \quad (10)$$

3.2 Contact analysis

In this example, the following constraints are imposed:

$$\begin{aligned} & n_R + n_S = 4 \\ & 2n_R + n_S < 7 \\ & \text{rank}(\boldsymbol{W}) = 2n_R + n_S \end{aligned} \quad (11)$$

The first constraint says that the total number of contacts is four. The next two constraints essentially make the problem determinate. In other words, a unique solution for the contact forces is directly available. Clearly, these conditions are satisfied for the following three cases: (a) $n_R = 2$, $n_S = 2$; (b) $n_R = 1$, $n_S = 3$; and (c)$n_R = 0$, $n_S = 4$.

The LCP model for any of the three cases can be derived by combining Eq.(8) and Eq.(10). This yields a $(2n_R + n_S) \times (2n_R + n_S)$ system given by:

$$\begin{bmatrix} \ddot{\phi}_{NR} \\ \ddot{\phi}_{TR} \\ \ddot{\phi}_{NS} \end{bmatrix} = \boldsymbol{A}_{RS} \begin{bmatrix} \boldsymbol{\lambda}_{NR} \\ \boldsymbol{\lambda}_{TR} \\ \boldsymbol{\lambda}_{NS} \end{bmatrix} + \boldsymbol{b}_{RS}, \quad (12)$$

where

$$\boldsymbol{A}_{RS} = \begin{bmatrix} \boldsymbol{W}_{NR}^T \\ \boldsymbol{W}_{TR}^T \\ \boldsymbol{W}_{NS}^T \end{bmatrix} \boldsymbol{M}^{-1} [\boldsymbol{W}_{NR} \ \boldsymbol{W}_{TR} \ \boldsymbol{W}_{\mu}],$$

$$\boldsymbol{b}_{RS} = \begin{bmatrix} \boldsymbol{W}_{NR}^T \\ \boldsymbol{W}_{TR}^T \\ \boldsymbol{W}_{NS}^T \end{bmatrix} \boldsymbol{M}^{-1} \left(\begin{bmatrix} \boldsymbol{g}_o \\ \boldsymbol{\tau} - \boldsymbol{g}_a \end{bmatrix} - \boldsymbol{h} \right) + \begin{bmatrix} \dot{\boldsymbol{W}}_{NR}^T \\ \dot{\boldsymbol{W}}_{TR}^T \\ \dot{\boldsymbol{W}}_{NS}^T \end{bmatrix} \dot{\boldsymbol{q}}.$$

As discussed in Section 2, there are three different scenarios for the simulation of the whole arm grasp. In the first scenario, Eq.(11) is satisfied and $\boldsymbol{A}_{RS}$ is a P-matrix. In this case the rigid body dynamic model is valid and solvable. The frictionless case, with $n_R = 0$, $n_S = 4$, is a special case in which $\boldsymbol{A}_{RS}$ is positive definite and both conditions are met. In the second scenario, Eq.(11) is satisfied, but there are no guarantees on $\boldsymbol{A}_{RS}$. In this case there is no unique solution for the contact forces and accelerations. This may happen for any of the three cases (a-c) above. Finally, in the third scenario, Eq.(11) is not satisfied. In this case, it is impossible to know what the contact forces are and therefore it is not possible to check for constraints on the contact forces. The $n_R = 4$, $n_S = 0$ case falls into this category. In the second and third scenarios, it is necessary to pursue a more complex model and as we argued before, the compliant contact model is the model of our choice. The next section illustrates our approach to integrating the two models.

4 Simulation approach and results

4.1 Approach to simulation

In Section 2, we discussed the advantages and disadvantages of both the LCP formulation and the compliant contact model. We propose an integrated approach to simulation that combines the strength of both models. The main idea is shown in Figure 4. The key step in this approach is to build the compliant contact state from the rigid body state variables when rigid body dynamics does not have a unique and stable solution for the contact forces [12]. However, during the switch from the LCP formulation to the compliant contact model, it is necessary to ensure that the state of the system and the dynamic model are continuous. This is done in the following way.

1. Use the gross motion of the rigid body system to compute the relative velocities at each contact point. In the case of grasping and manipulation tasks, for example, this can be given by Eq.(9).
2. Use the contact forces, $\boldsymbol{\lambda}_N$ and $\boldsymbol{\lambda}_T$, from the initial conditon or obtained by solving the LCP formulation from the previous time step, t_0, to construct the initial compliant contact state in both normal and tangential directions. For the ith contact in the normal direction,

$$\begin{aligned} \dot{\delta}_{N,i} &= -\dot{\phi}_{N,i}(\boldsymbol{q}) \\ \delta_{N,i} &= max\left\{0, \ \lambda_{N,i}^{-1}(\dot{\delta}_{N,i})\right\} \end{aligned}$$

where $\lambda_{N,i}^{-1}(\dot{\delta}_{N,i})$ is the inverse of the function $\lambda_{N,i}(\delta_{N,i}, \dot{\delta}_{N,i})$ in Eq.(6) for a given $\dot{\delta}_{N,i}$. In the tangential direction, if the ith contact is sliding at t_0, we assume that the the tangential deformation remains constant for the period of one time step of the integration process, which gives

$$\dot{\delta}_{T,i} = 0.$$

at $t = t_0$. If the contact is rolling,

$$\dot{\delta}_{T,i} = -\dot{\phi}_{T,i}(\boldsymbol{q}).$$

The tangential deformations for both rolling and sliding contacts are given by

$$\delta_{T,i} = \lambda_{T,i}^{-1}(\dot{\delta}_{T,i}).$$

Once the compliant contact state is built, as explained [5, 12], the compliant contact model allows the explicit calculation of the contact forces according to Eqs.(6,7) and the frictional constraints.

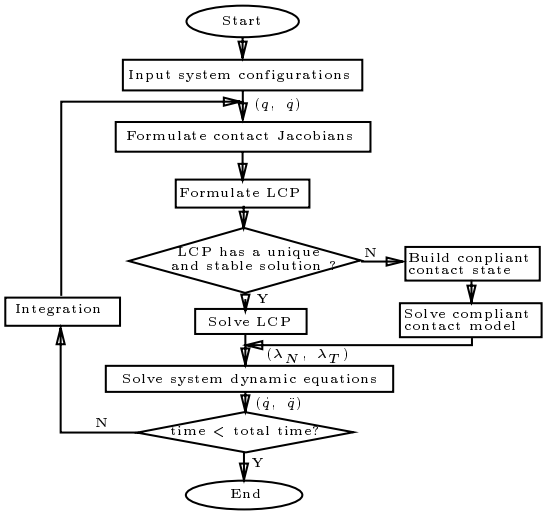

Figure 4: An integrated dynamic simulation approach for rigid body manipulations with frictional contacts

4.2 Simulation results

In this subsection, we will use the simulations of two frictional whole arm manipulation tasks to illustrate the use of the LCP model, the compliant contact model, and the integrated approach given above. In both tasks, the fingers of a two 2-DOF fingered hand is used to manipulate an elliptical object in the horizontal plane with sliding contacts. The configuration of the system is depicted in Figure 3. This is the $n_S = 4, n_R = 0$ scenario discussed in Section 3. The object has a major axis of 0.30m and its minor axis is 0.22m. The mass of the object is 1.69kg, and the moment of inertia about the center of mass is 1.46×10^{-2}kg·m^2. The fixed palm of the hand is 0.10m long. The length of each finger link is 0.20m. The mass of the finger link is 0.5kg with a centroidal moment of inertia of 1.67×10^{-3}kg·m^2.

The joints of the hand are driven by torque motors via a simple computed torque feedback law designed to manipulate the object along a desired trajectory. The details of the feedback law are explained in [16]. Although the grasp itself is statically indeterminate (four forces in the plane), because the torques are specified, the system is statically determinate. The rank of $\boldsymbol{W}_\mu \in \Re^{7\times4}$ remains four at all times. Since the system has three independent degrees of freedom, it is easy to verify that the grasped object can be manipulated in three independent directions.

For a frictionless task, the matrix $\boldsymbol{W}_{NS} \in \Re^{7\times4}$ is full rank and $\boldsymbol{W}_{NS}^T \boldsymbol{M}^{-1} \boldsymbol{W}_{NS}$ is symmetric and positive definite. Therefore the $\boldsymbol{A}$ matrix in the LCP formulation given by Eq.(5) is always a P-matrix, and hence the LCP formulation always has an unique solution for the contact forces. However, in the frictional case $\boldsymbol{A}$, expressed by $\boldsymbol{W}_{NS}^T \boldsymbol{M}^{-1} \boldsymbol{W}_\mu$, is no longer a guaranteed P-matrix. Whether $\boldsymbol{A}$ is a P-matrix or not depends on the configuration of the system, $\boldsymbol{q}$, as well as the coefficient of friction, $\boldsymbol{\mu}$, at the contact points.

We first consider the situation when the rigid body model has a unique solution throughout the duration of the simulation. We use this example to demonstrate and compare the performance of the rigid body model and the compliant contact model. In the second example, we show simulations for the case when difficulties of uniqueness and existence arise during a simulation by using the integrated approach.

The compliant contact model used in both examples is Kelvin-Voigt model with the following nondimensional form:

$$\boldsymbol{\lambda}_{N,T} = \frac{\bar{K}_{N,T}}{\epsilon \frac{t_0^2}{m_0}} \boldsymbol{\delta}_{N,T} + \frac{\bar{C}_{N,T}}{\sqrt{\epsilon} \frac{t_0}{m_0}} \dot{\boldsymbol{\delta}}_{N,T} \tag{13}$$

where $\bar{K}_{N,T}$ and $\bar{C}_{N,T}$ denote the dimensionless stiffness and damping ratio in the normal and tangential directions, respectively. m_0 is the characteristic mass and t_0 is the characteristic time. ϵ is a dimensionless scalar that represents the contact deformation scale [12]. In both examples $\bar{K}_{N,T} = \bar{C}_{N,T} = 1$, $t_0 = 1$sec, and $m_0 = m_o$ where m_o is the mass of the object.

Example 1: LCP has a unique solution The manipulation task is to rotate the object while keep its center of mass stationary. A fifth order polynomial is used to interpolate the orientation of the object. It can be shown that for this plan, if we choose $\mu = 0.1$ at all four contact points, the $\boldsymbol{A}$ matrix in the LCP formulation is always a P-matrix. The desired rotation of the object and the corresponding input joint torque history are shown in Figure 5.

The simulation results are provided for the rigid body LCP solution and for the compliant contact model for different values of ϵ (1×10^{-3}, 5×10^{-4}). The main point to be observed here is that the solution of the compliant contact model is seen to approach the LCP solution with decreasing values of ϵ. Figure 6 shows the snap shots of the simulation results for system configurations. Figure 7 shows the variation of the normal and tangential contact forces at each contact point. The manipulation task, which is to rotate the object from 70 degree to 110 degree in 1 second, can be simulated by either compliant model or the rigid body LCP model as depicted in

Figure 8(a). Figure 8(b) shows that the two models are in agreement within 1mm.

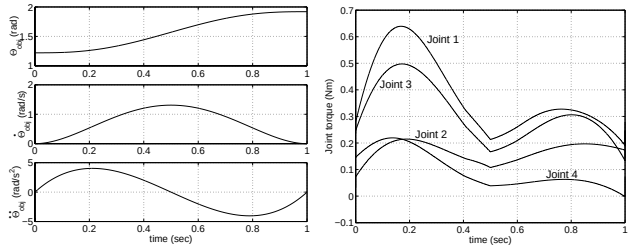

(a) Desired rotation (b) Input joint torques

Figure 5: An elliptical object being rotated counter clockwise with four sliding contacts.

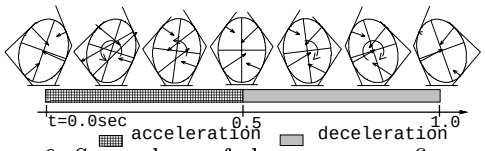

Figure 6: Snap shots of the system configuration.

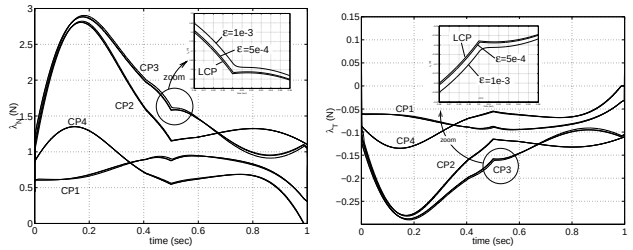

(a) Normal contact force. (b) Tangential contact force.

Figure 7: The contact force history by using both the rigid body LCP model and the compliant contact model (CP–Contact Point).

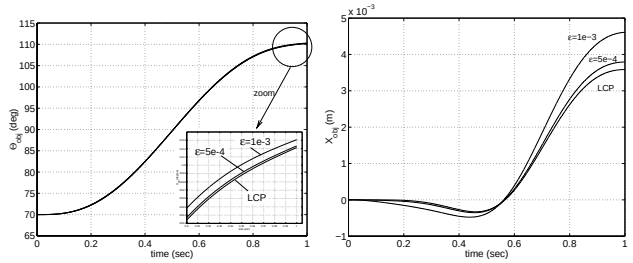

(a) Object orientation. (b) Horizontal displacement.

Figure 8: Trajectory of the object orientation, and variation of object position in the horizontal direction

Example 2: LCP does not always predict a unique solution In general, there is no guarantee the LCP formulation will have a unique solution for a frictional manipulation task. For example, consider the translation of the object from 0.12m to 0.18m in the vertical direction as depicted in Figure 9(a). The input torque history shown in Figure 9(b) is obtained through the same approach as in Example 1. If we set the coefficient of friction between the object and arm links 1 and 3 as $\mu_1 = 0.8$, and $\mu_2 = 0.6$ for links 2 and 4, we can show [17] that the P-matrix condition is not always satisfied during the task. For example, Figure 10 shows that at $t = 0.2$sec the chosen coefficient of friction falls into the P-matrix region while at $t = 0.5$sec it does not.

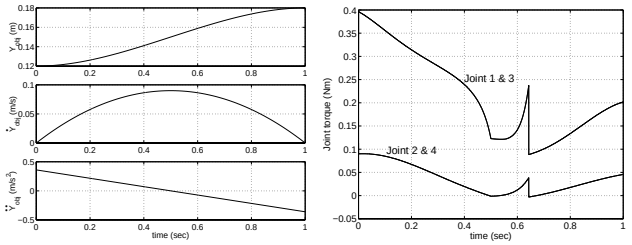

(a) Desired translation (b) Input joint torques

Figure 9: An elliptical object being translated in the positive y-direction with four sliding contacts.

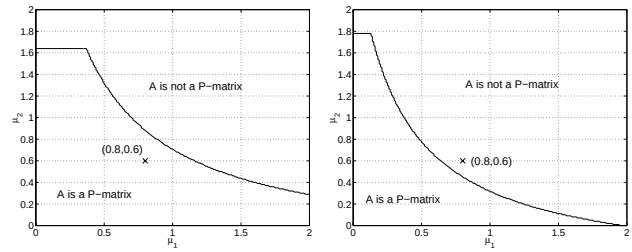

(a) t=0.2sec (b) t=0.5sec

Figure 10: μ-space plots for the manipulation task given by Figure 9 at different times.

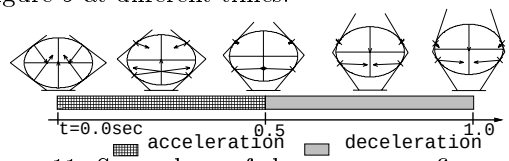

Figure 11: Snap shots of the system configuration.

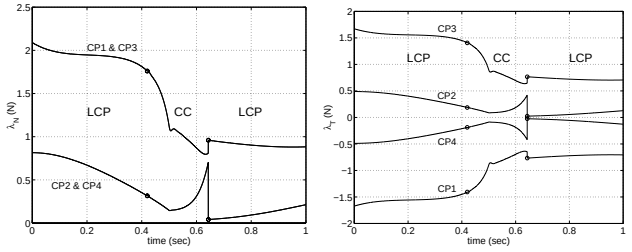

(a) Normal contact force. (b) Tangential contact force.

Figure 12: The contact force history.

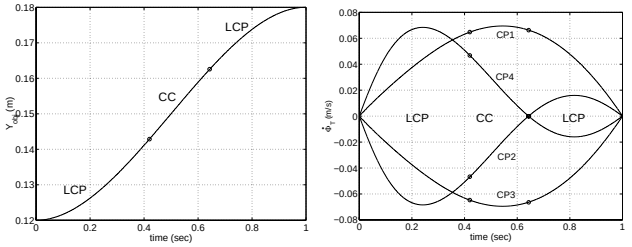

(a) (b)

Figure 13: Variations of (a) the object displacement in y-direction and (b) relative tangential velocities at the contact points.

The integrated approach proposed in the previous subsection is used to automatically switch the simulation flow between the rigid body LCP model and the CC (compliant contact) model based on the P-matrix criterion and the stability conditions. The results are

illustrated in Figures 11-13. The small circles on the plots indicate the switching points during the simulation. There are two points worth noting. First, the integrated approach enables a continuous transition for the system dynamics when switching between models. There are two switches in the simulation. The first one, at $t = 0.420sec$, is a switch from LCP to CC model. The second one, at $t = 0.643sec$, switches the simulation back to using the LCP model. Second, directions of the relative tangential velocities at contact points 2 and 4 change as shown in Figure 13(b). Since Coulomb's friction law is used, this change in direction causes a discontinuity in both the input joint torque trajectory and the contact force history.

5 Concluding remarks

It is well-known that there are difficulties in using rigid body dynamic models for the dynamic simulation of systems with frictional contacts. In particular, when rigid body models are used in conjunction with Coulomb friction for dynamic simulation of systems with frictional contacts, there may be situations in which there are no solutions or multiple solutions for the contact forces and the accelerations. On the other hand, a simple compliant contact model, when used with the rigid body dynamic equations of motion, always yields a unique solution for the accelerations and the forces. While this model is superior to the traditional rigid body model in terms of accuracy and robustness, it is also more complex and requires a larger number of parameters. Therefore, it is appealing to use rigid body models whenever concerns of uniqueness and existence do not arise.

In this paper, we proposed an approach to simulation that integrates the compliant contact model and the rigid body LCP model to maximize computational efficiency without compromising accuracy. This is done by using the rigid body model whenever possible and by switching to a compliant contact model when the equations show a potential problem with existence or uniqueness. We presented a range of examples to show that this method can be used to simulate any planar enveloping or whole arm grasps.

There are some obvious issues to consider in future research. First, the extension to three-dimensions, although straightforward from a conceptual standpoint, is difficult from a practical view point because of the frictional model and the tangential constraints. Second, the process of developing the state for the compliant contact model before a transition is based on the assumption that $\dot{\delta}_{T,i} = 0$ at each contact. Although this ensures a continuous transition between the two models, there is no physical basis for this assumption. If the rigid body dynamic model solution is stable [12], this erroneous assumption simply introduces a perturbation that gets damped out very quickly. Understanding the effect of such perturbations on the simulation results is a central focus of our ongoing work.

Acknowledgments

We gratefully acknowledge the support of NSF grants CISE RI 9703220, GRT 9355018, and MIP 9420397, and ARO grant MURI DAAH04-96-1-0007.

References

[1] R. W. Cottle, J. S. Pang, and R. E. Stone. *The Linear Complementarity Problem.* Academic Press, Inc., San Diego, CA, 1992.

[2] M. R. Cutkosky. *Robotic Grasping and Fine Manipulation.* Kluwer Academic Publishers, 1985.

[3] M. Erdmann. An exploration of nonprehensile two-palm manipulation. *Int'l Journal of Robotics Research*, 17:485–503, May 1998.

[4] W. S. Howard and V. Kumar. A minimum principle for the dynamic analysis of systems with frictional contacts. In *Proc. of the 1993 IEEE Int'l Conf. on Robotics and Automation*, volume 1, pages 437–442, 1993.

[5] P. R. Kraus, A. Fredriksson, and V. Kumar. Modeling of frictional contacts for dynamic simulation. In *Proceedings of IROS 1997 Workshop on Dynamic Simulation: Methods and Applications*, Sept. 1997.

[6] V. Kumar and K. J. Waldron. Force distribution in closed kinematic chains. *IEEE Journal of Robotics and Automation*, 4(6), Dec. 1988.

[7] P. Lötstedt. Analysis of some difficulties encountered in the simulation of mechanical systems with constraints. Technical report, NADA - The Royal Institute of Technology, Stockholm, Sweden, 1979. TRITA-NA-7914.

[8] M. T. Mason and Y. Wang. On the inconsistency of rigid-body frictional planar mechanics. In *Proc. of the 1988 IEEE Int'l Conf. on Robotics and Automation*, pages 524–528, 1988.

[9] N. H. McClamroch. A singular perturbation approach to modeling and control of manipulators constrained by a stiff environment. In *Proceedings of the 28th Conference on Decision and Control*, pages 2407–2411, Dec. 1989.

[10] B. Mirtich et al. Estimating pose statistics for robotic part feeders. In *Proc. of the 1996 IEEE Int'l Conf. on Robotics and Automation*, pages 1140–1146, 1996.

[11] K. Mirza and D. E. Orin. General formulation for force distribution in power grasp. In *Proc. of the 1994 IEEE Int'l Conf. on Robotics and Automation*, pages 880–887, 1994.

[12] P. Song, P. Kraus, V. Kumar, and P. Dupont. Analysis of rigid body dynamic models for simulation of systems with frictional contacts. Submitted to ASME Journal of Applied Mechanics, June 1999, 34 pages. Available at http://www.cis.upenn.edu/∼pengs/publications/jam99.ps.

[13] J. Trinkle, J.-S. Pang, S. Sudarsky, and G. Lo. On dynamic multi-rigid-body contact problems with coulomb friction. *Zeitschrift fr Angewandte Mathematik und Mechanik*, 77(4):267–280, Apr. 1997.

[14] C. Ullrich and D. K. Pai. Contact response maps for real time dynamic simulation. In *Proc. of the 1998 IEEE Int'l Conf. on Robotics and Automation*, pages 1950–1957, Leuven, Belgium, May 1998.

[15] Y.-T. Wang and V. Kumar. Simulation of mechanical systems with unilateral constraints. *ASME Journal of Mechanical Design*, 116(2):571–580, June 1994.

[16] M. Yashima and H. Yamaguchi. Control of whole finger manipulation utilizing frictionless sliding contact – theory and experiment. *Mechanism and Machine Theory*, 34:1255–1269, 1999.

[17] M. Yashima, H. Yamaguchi, and Y. Hirano. Transit motion analysis of enveloping grasp based on the linear complementarity problem. *Transactions of the Japan Society of Mechanical Engineers*, 65(635):210–217, 1998.